Temperature-Dependent Protein Dynamics: A Simulation-Based Probabilistic Diffusion-Vibration Langevin Description

Kei Moritsugu[†,‡] and Jeremy C. Smith*[,†]

Computational Molecular Biophysics, Interdisciplinary Center for Scientific Computing (IWR), University of Heidelberg, Im Neuenheimer Feld 368, 69120 Heidelberg, Germany, and Graduate School of Material Science, Nara Institute of Science and Technology (NAIST), 630-0192 Nara, Japan

Received: September 19, 2005; In Final Form: December 14, 2005

An enduring challenge in the understanding of internal protein motions is the effective separation and characterization of diffusive and vibrational dynamical components. To address this problem, here nanosecond molecular dynamics trajectories of myoglobin in aqueous solution, performed over a range of temperatures between 120 and 300 K, are subjected to principal component analysis, and the coordinate autocorrelation functions of the resulting principal modes are interpreted using a model combining damped Langevin vibration within potential wells and barrier-crossing diffusion between them. Both the vibrational frequency and the fraction of the mean-square fluctuation arising from vibrational motion undergo transitions with temperature at about 180 K. In contrast, the vibrational friction remains linear with temperature. The diffusional component of the mean-square fluctuation increases dramatically at the dynamical transition. The heights of the energy barriers between the potential wells are estimated, and the associated diffusion constants are calculated using Kramers' rate theory. Model functions of the frequency dependence of the frictional and diffusional quantities are obtained. The dynamic structure factor from the full molecular dynamics trajectory is well reproduced by the model. Overall, the results indicate that a global description of nanosecond temperature-dependent diffusion and vibrational internal protein dynamics can be obtained by applying the results of the present diffusion-vibration model to the vibrational motions obtained from a normal-mode analysis.

1. Introduction

Protein function is mediated by anharmonic internal dynamics on a rugged potential energy surface.[1,2] This motion can be simulated using the molecular dynamics (MD) method.[3] The atomic trajectories thus obtained involve complex multidimensional motions on a variety of lengths and time scales. A popular method for simplifying the analysis of complex MD trajectories is to make a quasi-harmonic approximation of the atomic positional fluctuations using principal component analysis (PCA).[4−7] PCA of MD trajectories has demonstrated that internal protein atomic mean-square fluctuations (MSFs) are dominated by a small number of large-amplitude PCA modes with nonquadratic equilibrium distributions. Anharmonic protein motion can be thus largely described in terms of dynamics along these large-amplitude PCA modes.

Information on the distributions and amplitudes of motions in protein must be completed with a description of the time dependence. To do this, various models of the velocity autocorrelation function (VACF) (and its memory function) have been employed.[8] In previous work[9] the Langevin equation[10−16] was applied to analyze VACFs from MD trajectories of a small globular protein, myoglobin. Vibrational frequencies and friction coefficients were obtained by fitting the MD-derived VACF to the Langevin model on a normal mode basis. This work furnished physical insight into the temperature and hydration dependence of vibrational protein dynamics. However, although the vibrational protein motion is well reproduced by this Langevin model, the slow, diffusive motion in the protein is not represented. This difficulty originates from the complexity of protein dynamics and the wide range of time scales involved, i.e., the combination of fast ($<\sim 10^{-11}$ s) vibrations with relatively infrequent transitions between conformational substates involving the crossing of energy barriers.[1,2] Ensemble averaging renders the VACF relatively insensitive to rapid but rare barrier-crossing motions, and thus the VACF describes mostly the vibrational motion averaged over the potential wells explored during MD trajectories.

The difficulty in probing diffusive motion can be overcome by using the coordinate autocorrelation function (CACF). The large-amplitude, diffusive coordinate variations are manifested by slow damping of this ensemble-averaged function and are not masked by the small-amplitude vibrations. Here, we propose and perform modeling of the CACF for proteins. A simplified model of the CACF is constructed comprising both vibrational and diffusional components. This model is fitted to the small number of dominant, large-amplitude PCA modes for myoglobin. This enables a physical interpretation of the dynamics over the potential energy surface (PES) along each PCA mode in terms of a combination of vibrations within potential wells and diffusion between them (schematized in Figure 1).

By comparison of the model parameters obtained from MD trajectories at different temperatures, the temperature dependence of protein dynamics is analyzed. The dynamical "glass" transition has been characterized by the appearance of diffusive (nonvibrational) motion above the dynamical transition temperature of $T_g \sim 180-220$ K.[17−19] The present model allows the diffusional component of the MSF to be determined separately as a function of temperature, thus clarifying our picture of the dynamical transition.

* To whom correspondence may be addressed. Tel: +49-6221-54-8857. Fax: +49-6221-54-8868. E-mail: biocomputing@iwr.uni-heidelberg.de.
† University of Heidelberg.
‡ Nara Institute of Science and Technology.

10.1021/jp055314t CCC: $33.50
Published on Web 03/01/2006

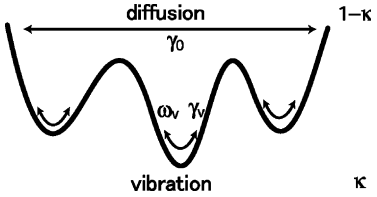

Figure 1. Schematic drawing of potential energy surface with associated model parameters from eq 13.

Diffusion originates in escapes from vibrational potential wells. The escape rate, i.e., the transition probability, is quantified here using Kramers' rate theory.[20] The present model is applied to estimation of the heights of potential energy barriers between the wells together with the probability of transition over the barriers and the associated diffusion constant. The estimated diffusion constant is then used for constructing the model functions of parameters, allowing protein dynamics to be reproduced via the present model combined with the simple model parameter functions thus obtained.

We also examine here the validity of the CACF model by calculating inelastic neutron scattering spectra, which are directly determined by the picosecond time scale atomic dynamics. The analysis allows an understanding of the relation between low-frequency vibrations and diffusion in internal protein dynamics to be deepened.

2. Methods

2.1. Dynamical Simulations. The data to which the coordinate autocorrelation function model was fitted were derived using molecular dynamics simulations and principal component analyses of carboxymyoglobin (Protein Data Bank structure 1A6G[21]) in aqueous solution. The model system was constructed as follows: A rectangular primary simulation box was built of dimensions 56 Å × 52 Å × 41 Å. A total of 3090 TIP3P water molecules[22] and 1 chloride counterion were placed in the box, explicitly solvating the myoglobin molecule, leading to an electrically neutral system of 11 780 atoms. Periodic boundary conditions were imposed on the box.

The simulations were performed using the program CHARMM, version 30b2.[23] The CHARMM all-atom parameter set 22[24] was used for the potential function. Electrostatic interactions were calculated using the particle-mesh Ewald method[25,26] with a dielectric constant of 1. The real space summation was truncated at 12 Å using $\kappa = 0.23$ Å^{-1}.

Separate simulations were carried out at constant temperatures 120, 150, 160, 170, 180, 190, 200, 210, 220, 230, 240, 250, 280, and 300 K and under constant pressure (1 atm) conditions (the NPT ensemble). To do these, the system was energy minimized with 1000 steps of the steepest descent method followed by 2000 steps of adopted basis Newton−Raphson minimization.[23] Then, each simulation system was uniformly heated to the target temperature during 30 ps and equilibrated for 100 ps with velocity scaling in the NVE ensemble and another 200 ps in the NPT ensemble. The temperature and pressure were controlled using the Nosé−Hoover algorithm[27,28] with mass parameters of $Q_T = 1000$ amu and $Q_P = 500$ amu, respectively. All production runs were performed for 1 ns. Both the atomic coordinates and velocities were saved every 50 fs for analysis.

Principal component analysis was performed on each simulation. For this, the mass-weighted myoglobin atom coordinates of the 1 ns MD production trajectories were fitted to one reference coordinate set for calculating the variance−covariance matrixes of the interatomic fluctuations. The matrixes obtained were diagonalized, leading to a set of uncorrelated harmonic distribution functions—the principal components. Each principal component mode has a mean-square fluctuation as its eigenvalue and an atomic displacement vector as its eigenvector. The PCA modes were arranged in descending order of their amplitudes.

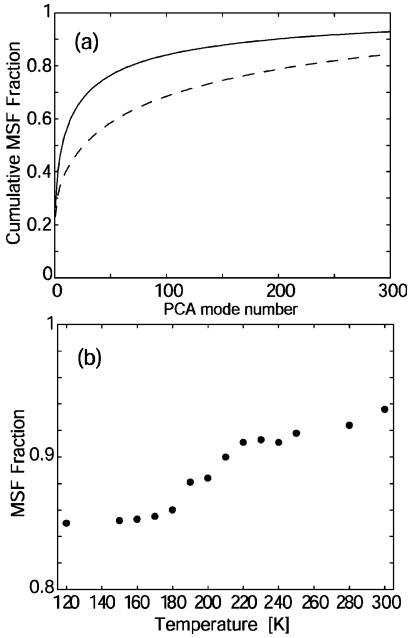

Figure 2. Ratio of MSF of selected PCA modes to the total MSF. (a) Cumulative contribution is plotted as a function of PCA mode number at 300 K (solid curve) and at 120 K (dashed curve). (b) MSF fraction of the 300 largest-amplitude PCA modes to the total MSF as a function of temperature.

2.2. Coordinate Autocorrelation Function Model. The multidimensional protein motions were decomposed into one-dimensional motion along each PCA mode, which was subsequently analyzed using a model of the coordinate autocorrelation function. The 300 largest-amplitude PCA modes were examined, which account for more than 85% of the total mean-square fluctuations. The ratios of the cumulative MSF of the PCA modes to the total MSF are plotted in Figure 2a. The MSF fraction accounted for by a given number of PCA modes is larger at 300 K than at 120 K. The fraction of the dynamics represented by the 300 lowest PCA modes is shown as a function of temperature in Figure 2b. These modes dominate the MSF more strongly with increasing temperature. These results imply that the large-amplitude, diffusive motions make a larger relative contribution at higher temperature.

The dynamics along each PCA mode is modeled here as the combination of a fast (f) and a slow (s) dynamical component, i.e., the PCA coordinate is described as $x = x_f + x_s$ and the associated velocity as $v = v_f + v_s$. These motions are consistent with a hierarchical potential energy surface comprising a sequence of narrow potential wells on a broad PES curvature (schematized in Figure 1); i.e., fast vibration in the potential wells occurs together with slow motion between them. Assuming that the two elements are governed by two-dimensional Langevin dynamics with associated frictions and harmonic potential curvatures, the equations of motions are written as follows[10]

$$\frac{d^2}{dt^2} x_i + \sum_j (K_{ij} x_j + \gamma_{ij} \dot{x}_j) = R_i(t) \qquad (1)$$

$$(i, j) = (\mathrm{f}, \mathrm{s})$$

where K_{ij} is the second-derivative matrix that quantifies the

curvature of the harmonic potential energy surface, and $R_f(t)$ and $R_s(t)$ are random forces with Gaussian white noises that satisfy the following averages:

$$\langle R_i(t)\rangle = 0$$
$$\langle R_i(0)\, R_j(t)\rangle = 2\beta^{-1}\zeta_{ij}\delta(t) \qquad (2)$$
$$(i, j) = (\mathrm{f}, \mathrm{s})$$

The random force originates from the interactions with both the other protein principal component modes and the surrounding water molecules.

The motions, governed by stochastic processes with random forces, can be represented by the moments of the probability distributions of the coordinates and velocities. The distribution, $P(x,v,t|x_0,v_0,t_0)$, given the initial conditions of $x = x_0$ and $v = v_0$ at $t = t_0$, is derived using the distributions of fast and slow elements, $P(\alpha,t|\alpha_0,t_0)$, where $\alpha = (x_f,x_s,v_f,v_s)^t$, giving

$$P(x,v,t|x_0,v_0,t_0) = \int \mathrm{d}\alpha\, P(\alpha,t|\alpha_0,t_0)\delta(x - x_f - x_s)\delta(v - v_f - v_s) \quad (3)$$

$P(\alpha,t|\alpha_0,t_0)$ is determined by the Fokker−Planck equation in phase space[10,29] as follows:

$$\frac{\partial P(\alpha,t|\alpha_0,t_0)}{\partial t} = \left(-\mathbf{A}\frac{\partial}{\partial\alpha}\alpha + \mathbf{B}\frac{\partial^2}{\partial^2\alpha}\right)P(\alpha,t|\alpha_0,t_0) \qquad (4)$$

$$\mathbf{A} = \begin{pmatrix} 0 & 1 \\ -\mathbf{K} & -\gamma \end{pmatrix}, \qquad \mathbf{B} = \beta^{-1}\begin{pmatrix} 0 & 0 \\ 0 & \gamma \end{pmatrix}$$

The solution of eq 4 is well-known to be the Gaussian distribution

$$P(\alpha,t|\alpha_0,t_0) = \frac{1}{(2\pi)^4[\det \boldsymbol{\sigma}(t)]^{1/2}} \times \exp\left[-\frac{1}{2}(\alpha - \mathrm{e}^{\mathbf{A}t}\alpha_0)^t\boldsymbol{\sigma}^{-1}(t)(\alpha - \mathrm{e}^{\mathbf{A}t}\alpha_0)\right] \quad (5)$$

where the variance of the distribution, $\boldsymbol{\sigma}(t)$, satisfies

$$\dot{\boldsymbol{\sigma}}(t) = \mathbf{A}\boldsymbol{\sigma}(t) + \boldsymbol{\sigma}(t)\mathbf{A}^t + 2\mathbf{B} \qquad (6)$$

The matrix of correlation functions is thus given by

$$\mathbf{C}(t) = \mathrm{e}^{\mathbf{A}t}\boldsymbol{\sigma}(\infty) \qquad (7)$$

Here, the matrices of $\mathbf{K}$ and γ are assumed to be diagonal; i.e., the fast and slow motions are assumed uncorrelated. This assumption is valid when the magnitudes of the two vibrational frequencies, ω_f and ω_s (i.e., the diagonal elements of $\mathbf{K}$ are ω_f^2 and ω_s^2) are very different. The variances of x and v are then decomposed as $\langle x^2\rangle = \langle x_f^2\rangle + \langle x_s^2\rangle$ and $\langle v^2\rangle = \langle v_f^2\rangle + \langle v_s^2\rangle$, using the law of equipartition, which states that the equilibrium kinetic and potential energies are equal in the harmonic system. The following relations are derived

$$\langle v_f^2\rangle = \omega_f^2\langle x_f^2\rangle = \eta\langle v^2\rangle$$
$$\langle v_s^2\rangle = \omega_s^2\langle x_s^2\rangle = (1 - \eta)\langle v^2\rangle \qquad (8)$$

where η is therefore the fast-element fraction of the mean-square velocity fluctuation, i.e., $\eta = \langle v_f^2\rangle/\langle v^2\rangle = \langle v_f^2\rangle/[\langle v_f^2\rangle + \langle v_s^2\rangle]$. The equilibrium distribution is then written as

$$\beta\boldsymbol{\sigma}(\infty) = \begin{pmatrix} \eta/\omega_f^2 & 0 & 0 & \\ 0 & (1-\eta)/\omega_s^2 & & \\ & 0 & \eta & 0 \\ & & 0 & 1-\eta \end{pmatrix} \qquad (9)$$

$\mathbf{C}(t)$ can be calculated from eqs 7 and 9 using η. Defining κ as the fast-element fraction of the mean-square coordinate fluctuation, i.e., $\kappa = \langle x_f^2\rangle/\langle x^2\rangle = \langle x_f^2\rangle/[\langle x_f^2\rangle + \langle x_s^2\rangle] = (\eta/\omega_f^2)/[\eta/\omega_f^2 + (1 - \eta)/\omega_s^2]$, the scaled coordinate and velocity autocorrelation functions are given by

$$\psi_{coo}(t) = \frac{\langle x(0)x(t)\rangle}{\langle x^2\rangle} = \kappa\frac{\langle x_f(0)x_f(t)\rangle}{\langle x_f^2\rangle} + (1 - \kappa)\frac{\langle x_s(0)x_s(t)\rangle}{\langle x_s^2\rangle} \qquad (10)$$

$$\psi_{vel}(t) = \frac{\langle v(0)v(t)\rangle}{\langle v^2\rangle} = \eta\frac{\langle v_f(0)v_f(t)\rangle}{\langle v_f^2\rangle} + (1 - \eta)\frac{\langle v_s(0)v_s(t)\rangle}{\langle v_s^2\rangle} \qquad (11)$$

Equations 10 and 11 show that the fractions of the vibrational motion (η and κ) are different in the CACF and the VACF. η is likely to be nearly 1 as a result of the ensemble average because the barrier-crossing motions between conformational substates are less frequent compared to the vibrational period.[9] However, κ is expected to be significantly lower than 1 because $\omega_s^2 \ll \omega_f^2$ and thus $(1 - \eta)/\omega_s^2 \approx \eta/\omega_f^2$—this encapsulates the advantage of introducing the CACF into the analysis.

The VACF and CACF for Langevin dynamics are derived elsewhere.[12,13] In the previous study of the VACF model,[9] the velocity autocorrelation function was modeled as a single damped Langevin oscillator, i.e., using $\eta \approx 1$, giving

$$\psi_{vel,model}(t) = \begin{cases} \exp(-\gamma_v t/2)\left(\cos\varpi_v t - \dfrac{\gamma_v}{2\varpi_v}\sin\varpi_v t\right) & \gamma_v < 2\omega_v \\ \dfrac{-\gamma_v/2 + \varpi_{v0}}{2\varpi_{v0}}\mathrm{e}^{(-\gamma_v/2+\varpi_{v0})t} + \dfrac{\gamma_v/2 + \varpi_{v0}}{2\varpi_{v0}}\mathrm{e}^{(-\gamma_v/2+\varpi_{v0})t} & \gamma_v \geq 2\omega_v \end{cases} \qquad (12)$$

where ω_v and γ_v are the vibrational frequency and friction, and $\varpi_v = (\omega_v^2 - \gamma_v^2/4)^{1/2}$ is the effective frequency for underdamped vibrational motion ($\gamma_v < 2\omega_v$) and $\varpi_{v0} = (\gamma_v^2/4 - \omega_v^2)^{1/2}$ holds for overdamped motion ($\gamma_v \geq 2\omega_v$).

In the present study of the CACF model, we make an approximation that the curvature of the potential governing by the slow element, ω_s, is zero; i.e., the slow motion is modeled as simple diffusion (with a friction coefficient of γ_0) on a flat PES. Furthermore, in the case that the fast, vibrational motion is overdamped, i.e., when the damping is faster than the vibrational frequency, then $\psi_{coo}(t)$ is modeled as the combination of two simple diffusive motions. An alternative to this model would be to apply the overdamped description of the Langevin model, but this would risk overfitting by using a three-exponential model function. Indeed, trial fits showed that a three-exponential model provides little fitting improvement relative to the two-exponential model (results not shown).

The resulting model CACF is as follows

$$\psi_{\mathrm{coo,model}}(t) = \begin{cases} \kappa\left[\exp(-\gamma_v t/2)\left(\cos \varpi_v t + \frac{\gamma_v}{2\varpi_v}\sin \varpi_v t\right)\right] + (1-\kappa)\frac{1-\exp(-\gamma_0 t)}{\gamma_0 t} & \gamma_v < 2\omega_v \\ \kappa\frac{1-\exp(-\gamma_v t)}{\gamma_v t} + (1-\kappa)\frac{1-\exp(-\gamma_0 t)}{\gamma_0 t} & \text{otherwise} \end{cases} \quad (13)$$

where $\varpi_v = (\omega_v^2 - \gamma_v^2/4)^{1/2}$ is the effective frequency for underdamped vibrational motion ($\gamma_v < 2\omega_v$). Both model functions in eq 13 were fitted to the simulation-derived coordinate autocorrelation function, $\psi_{\mathrm{coo,MD}}(t)$, over the range of $t = 0-L$, with L being from 5 to 20 ps depending on the damping rate of $\psi_{\mathrm{coo,MD}}(t)$ of the corresponding PCA mode. Then the integrals of the square deviation between the MD and model CACF, i.e., $\int_0^T \mathrm{d}t|\psi_{\mathrm{coo,\,MD}}(t) - \psi_{\mathrm{coo,\,model}}(t)|^2$ were calculated for both models as an evaluation function, allowing the associated dynamics to be determined. The square deviations between the MD-derived and the fitting CACF quantify the errors of the obtained parameters.

By fitting the MD-derived CACF to eq 13, the vibrational fraction (κ), the vibrational frequency and friction (ω_v and γ_v), and the diffusion damping coefficient (γ_0) were determined for each PCA mode. These model parameters are related to characteristics of the PES shown in Figure 1. These quantities were averaged over the large-amplitude PCA modes, and their temperature dependence was analyzed.

The CACF model makes possible the decomposition of the protein dynamics along each PCA mode into vibrational and diffusional contributions. The vibrational and diffusional mean-square fluctuations along each PCA mode can be calculated using κ and the MSF of mode n (obtained as its eigenvalue, λ_n, i.e., $\langle x_n^2\rangle = \lambda_n$) as $\kappa_n\lambda_n$ and $(1 - \kappa_n)\lambda_n$, respectively. A characteristic of the present model is decomposition into diffusion and vibration through a probabilistic description (i.e., κ is between 0 and 1) owing to dynamical aspects, rather than a deterministic description (i.e., κ is 0 or 1) as would be obtained using only the equilibrium potential of mean force.[6,30]

2.3. Dynamic Structure Factor. The neutron scattering incoherent dynamic structure factor, $S(\mathbf{q},\omega)$, was calculated as the time Fourier transform of incoherent intermediate scattering function, $F(\mathbf{q},t)$

$$S(\mathbf{q},\omega) = \frac{1}{2\pi}\int F(\mathbf{q},t)\mathrm{e}^{-i\omega t}\,\mathrm{d}t \quad (14)$$

$F(\mathbf{q},t)$ in the classical limit was calculated directly from the MD trajectories using the following equation[31-33]

$$F(\mathbf{q},t) = \sum_{i=1}^{N} b_{\mathrm{inc},i}{}^2\langle \mathrm{e}^{-i\mathbf{q}\cdot\mathbf{r}_i(0)}\,\mathrm{e}^{i\mathbf{q}\cdot\mathbf{r}_i(t)}\rangle \quad (15)$$

where $b_{\mathrm{inc},i}{}^2$ is the square of the isotopic incoherent scattering length of atom i. In these calculations, $q = |\mathbf{q}|$ was set to 2 Å^{-1} and averaged over three orthogonal directions. The energy resolution function was assumed to be a Gaussian with variance, $\Delta E = 30$ μeV, which corresponds to a typical experimental instrumental energy resolution.[34] For the spectra calculated from the MD simulations, 2^{16} trajectory frames separated by 10 fs (total length of ~640 ps) were used.

The incoherent intermediate scattering function in the classical form was also calculated analytically using the CACF model in eq 13 as[35,36]

$$F(\mathbf{q},t) = \sum_{i=1}^{N} b_{\mathrm{inc},i}{}^2 \exp\left\{-\sum_{n=1}^{M}\frac{\lambda_n}{m_i}\left|\mathbf{q}\cdot\mathbf{u}_n{}^{(i)}\right|^2[1-\varphi_{\mathrm{coo},n}(t)]\right\} \quad (16)$$

where M is the number of PCA modes considered and $\mathbf{u}_n{}^{(i)}$ is the displacement of atom i in the eigenvector of mode n. To do this, the 300 largest-amplitude PCA modes ($n = 1-300$) with the CACF fitting model in eq 13 were used as well as the second-largest 1700 PCA modes ($n = 301-2000$) with the VACF fitting model in eq 12 (i.e., $\kappa = 1$ is assumed in eq 13), i.e., $M = 2000$.

3. Results and Discussion

3.1. Coordinate and Velocity Autocorrelation Functions from Molecular Dynamics Trajectories. Figures 3 and 4 show time series of coordinates and velocities for selected principal component modes together with their associated autocorrelation functions obtained from the MD trajectory at 300 K in solution. In modes 1 and 8, the distributions and the time correlation functions of the coordinates are qualitatively different from those of the velocities, indicating the presence of complex motion with both fast and slow time scales. For these modes the CACF exhibits slow variation via diffusion, in contrast to the fast

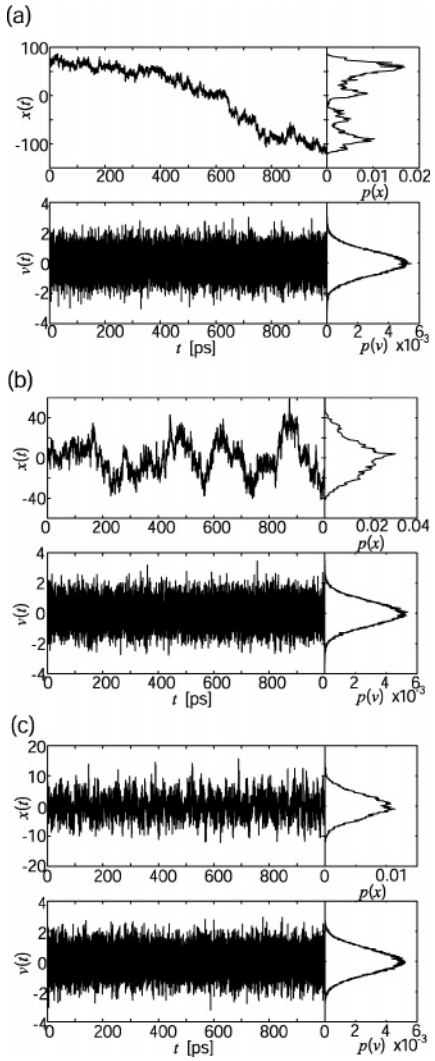

Figure 3. Time series of coordinates (upper left) and velocities (lower left) of PCA modes from MD trajectory at 300 K: (a) mode 1, (b) mode 8, and (c) mode 100. The associated probability distributions are shown in the right panels.

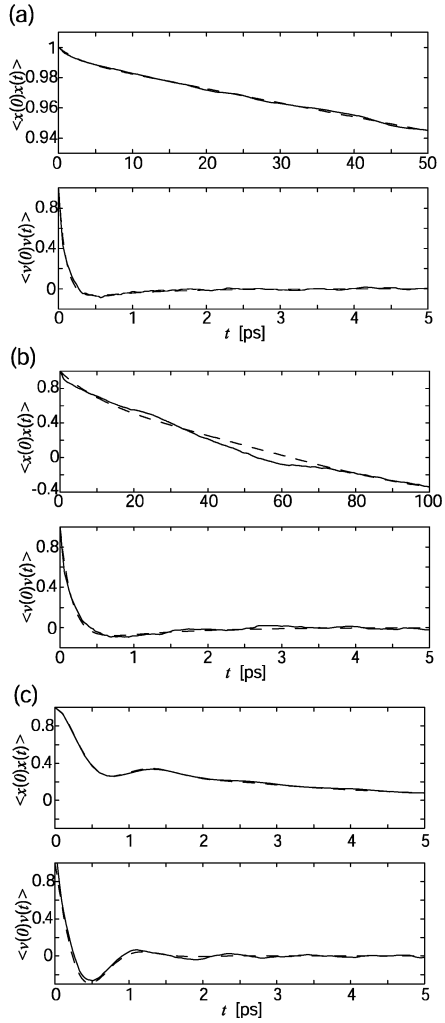

Figure 4. Scaled coordinate (upper) and velocity (lower) autocorrelation functions of PCA modes obtained from MD trajectory at 300 K: (a) mode 1, (b) mode 8, and (c) mode 100. Fits of eqs 12 and 13 are shown as dashed curves.

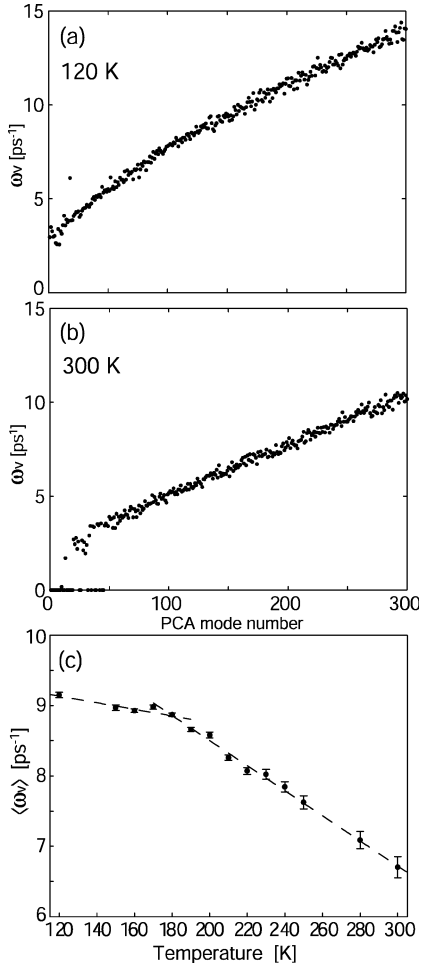

Figure 5. Vibrational frequency, ω_v, as a function of PCA mode number, derived from MD trajectories (a) at 120 K and (b) at 300 K. In (c) the average of ω_v over the 300 largest-amplitude PCA modes is plotted as a function of temperature. Linear fits are shown as dashed lines.

damping of the VACF which is dominated by vibrational motion governed by a harmonic (Gaussian) velocity distribution. In mode 100 both the coordinate and velocity distributions are harmonic. Interestingly, however, in mode 100 the associated CACF and VACF have quite different time courses. The CACF exhibits an exponential-like damping (∼10 ps) in addition to a damped oscillation that has a period similar to that of the VACF (∼1 ps). Both autocorrelation functions for mode 100 were well fitted by eqs 12 and 13, showing the validity of these model functions derived from Langevin vibration combined with simple diffusion. In this way, the analysis via the CACF makes possible the representation of the diffusive dynamics.

3.2. Calculations of the Model Parameters: Temperature Dependence. The CACF along each PCA mode was calculated from the MD trajectories in solution at various temperatures, followed by fitting the MD-derived CACF to the model functions in eq 13. The calculated model parameters were examined in order to obtain physical insight into the temperature dependence of protein internal dynamics.

In Figures 5a and 5b the vibrational frequencies of PCA modes, ω_v, from the MD simulations at 120 and at 300 K are shown. The larger-amplitude PCA modes (with smaller PCA mode numbers) have smaller ω_v, indicating broader curvature of the associated vibrational potential wells. At 300 K the vibrational frequencies are lower than those at 120 K, due to PES broadening via increased anharmonicity.[9] A few of the largest-amplitude PCA modes at 300 K have frequencies close to zero, due to the difficulty of fitting the CACF model of eq 13 at very small κ, i.e., when the large-amplitude diffusive motions dominate and the small-amplitude vibrations contribute little to the CACF.

To further examine the temperature dependence the average of ω_v over the 300 largest-amplitude PCA modes

$$\langle\omega_v\rangle = \sum_{n=1}^{300} \omega_{v,n}/300$$

was calculated for each temperature, T. $\langle\omega_v\rangle$ (T) in Figure 5c shows a transition at $T \sim 180$ K, corresponding to a rapid broadening of the potential wells. The transition temperature is in the range of the protein glass transition temperature, at which the diffusive motions are activated.[17−19]

The vibrational friction coefficients, γ_v, from the MD simulations at 120 and at 300 K are shown in Figures 6a and 6b. γ_v increases with ω_v, indicating increased interaction of protein PCA modes with high-frequency protein motions via frequency resonance.[9,37,38] γ_v is generally larger at 300 K than at 120 K due to more rugged potential wells via stronger anharmonicity.[9] The width of the distribution of γ_v is broader

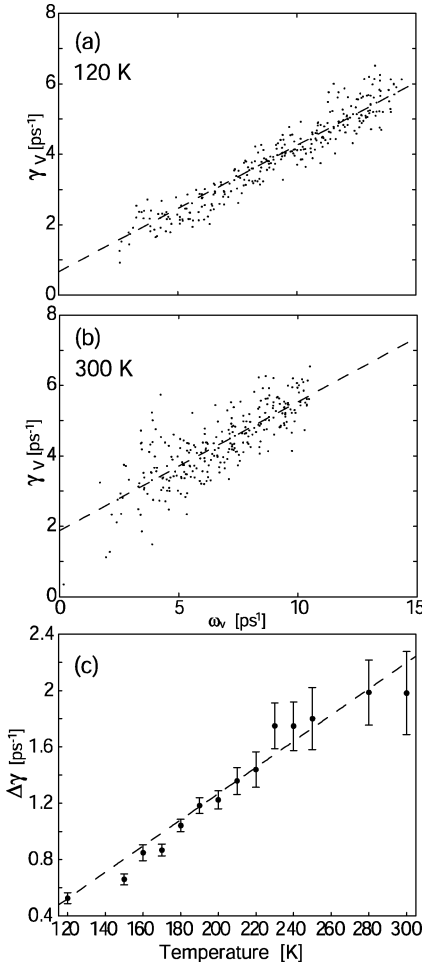

Figure 6. Vibrational friction, γ_v, as a function of vibrational frequency, ω_v, derived from MD trajectories (a) at 120 K and (b) at 300 K. In (c) $\Delta\gamma$ (see text in detail) is plotted as a function of temperature. Linear fits are shown as dashed lines.

at higher temperatures, reflecting larger deviations from the average friction due to a larger heterogeneity of vibrational motions.

The distributions in Figures 6a and 6b were fitted by linear functions, $\gamma_v = A\omega_v + \Delta\gamma$, which are also shown in the figures. The slopes, A, are 0.375 in both cases, indicating temperature independence. The coefficient, $\Delta\gamma$, i.e., the zero-frequency friction, does not correspond to the slow damping coefficient, γ_0. Rather, this determines the critical frequency of the vibrational motion, $\omega_{v,c} = \gamma_{v,c}/2$, i.e., $\omega_{v,c} = \Delta\gamma/(2 - A)$. At frequencies lower than $\omega_{v,c}$ the motion becomes overdamped. $\Delta\gamma$ is plotted in Figure 6c as a function of temperature and is seen to increase linearly. Thus, the ~180 K transition has no visible effect on the vibrational friction, which characterizes the roughness of vibrational potential wells, and is apparently independent of the diffusive, barrier-crossing motions.

In Figures 7a and 7b are shown the vibrational fractions, κ, from the MD simulations at 120 and at 300 K. With decreasing amplitude of the PCA modes (increasing PCA mode number) κ increases and becomes close to 1, i.e., purely vibrational. At 120 K κ is close to 1 for all but a few of the largest-amplitude PCA modes, confirming the dominance of vibrational motion at this low temperature. At 300 K, in contrast, κ is below 0.6 for most of the 300 largest-amplitude modes, showing the strong presence of diffusive motions in addition to vibrations. The average of κ over the 300 largest-amplitude PCA modes

$$\langle\kappa\rangle = \sum_{n=1}^{300} \kappa_n/300$$

shown in Figure 7c exhibits a clear transition at $T \sim 180$ K, corresponding to a rapid enhancement of the diffusive motions. The rate of decrease of $\langle\kappa\rangle$ becomes smaller at higher temperature due to the convergence of $\langle\kappa\rangle$ toward 0, rather than to other dynamical contributions.

The CACF decomposition into vibrational and diffusional contributions is now applied to the mean-square fluctuation. To do this the vibrational and diffusional mean-square fluctuations of each PCA mode were separately calculated and summed over $N_{85\%}$ of the largest-amplitude PCA modes, i.e., those accounting for ~85% of the total MSF, as follows

$$\langle x^2\rangle_{vib} = \sum_{n=1}^{N_{85\%}} \langle x_n^2\rangle_{vib} = \sum_{n=1}^{N_{85\%}} \lambda_n\kappa_n$$

$$\langle x^2\rangle_{diff} = \sum_{n=1}^{N_{85\%}} \langle x_n^2\rangle_{diff} = \sum_{n=1}^{N_{85\%}} \lambda_n(1-\kappa_n) \qquad (17)$$

The results are shown in Figure 8. The vibrational MSF increases linearly with temperature, i.e., with the kinetic energy of the system. This linear increase is characteristic of harmonic dynamics. In contrast, the diffusional MSF undergoes a transi-

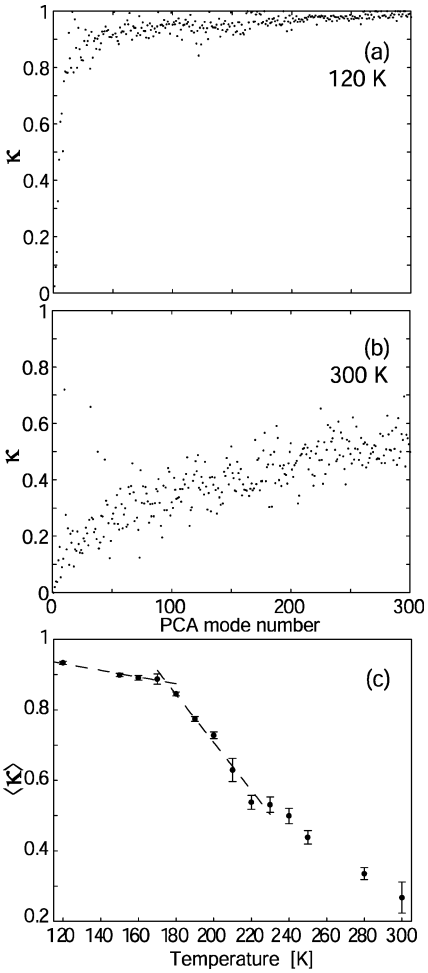

Figure 7. Vibrational fraction, κ, as a function of PCA mode number, derived from MD trajectories (a) at 120 K and (b) at 300 K. In (c) the averages of κ over the 300 largest-amplitude PCA modes are plotted as a function of temperature. Linear fits are shown as dashed lines.

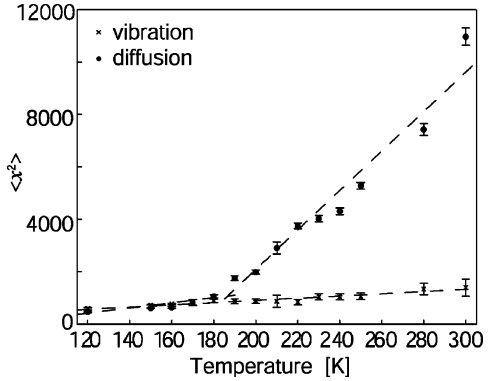

Figure 8. Sum of mean-square fluctuation, $\langle \Delta x^2 \rangle$, over those largest-amplitude PCA modes accounting for 85% of the total mean-square fluctuations as a function of temperature: The contributions of the diffusion and vibration are plotted with dots and crosses, respectively. The error bars of both quantities are equal because these sums are the eigenvalues of PCA, irrespective of the fitting procedures. Linear fits are shown as dashed lines.

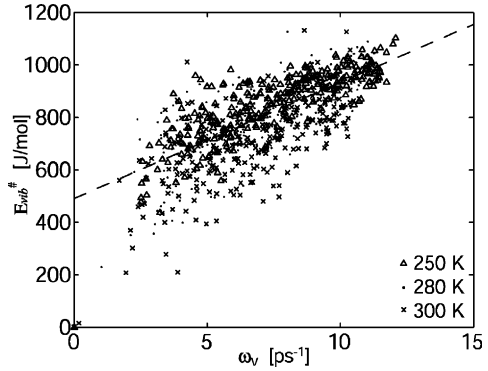

Figure 9. Potential energy barrier of the vibrational potential wells, $\Delta E^{\ddagger}$, as a function of vibrational frequency, ω_v, derived from MD trajectories at 250 K (triangle), at 280 K (dot), and at 300 K (cross). Linear fit is shown as dashed line.

tion at $T \sim 180$ K, indicating a strong enhancement of the diffusive motions above the glass-transition temperature.

3.3. Model Functions of Parameters: Estimation of Diffusional Contribution. The heights of the potential energy barriers between the vibrational potential wells are now estimated. The probabilities of transition over the barriers are then calculated from the obtained barrier heights using Kramers' rate theory, allowing the associated diffusion constant to be estimated. The diffusional contribution thus obtained is used for constructing the model functions of the parameters in eq 13 using only the vibrational frequency.

First, the heights of the potential energy barriers, $\Delta E^{\ddagger}$, are considered. It is assumed that the vibrational amplitudes correspond to the barrier heights, i.e., the vibrational potential wells can be approximated as harmonic. $\Delta E^{\ddagger}$ is then derived as

$$\Delta E_n^{\ddagger} \approx \frac{1}{2}\omega_{v,n}^2 \langle x_n^2 \rangle_{vib} = \frac{1}{2}\omega_{v,n}^2 \kappa_n \lambda_n \qquad (18)$$

The vibrational amplitudes can be evaluated only when the MD trajectories explore the full-amplitude vibrational potential wells, i.e., $\kappa < 1$, where diffusive motions between vibrational potential wells exist. Figure 9 shows the distributions of $\Delta E^{\ddagger}$ as a function of the vibrational frequencies, ω_v, at the three highest temperatures (250, 270, and 300 K), i.e., for which $\kappa < 1$ is satisfied. $\Delta E^{\ddagger}$ decreases with decreasing ω_v, meaning that escape from the vibrational potential wells is more likely to occur from lower frequency modes. The three distributions are almost the same, and each can be approximately fitted by the linear function, $\Delta E^{\ddagger}(J) = 44.2\omega_v\ (\mathrm{ps}^{-1}) + 491$, shown also in Figure 9. The approximately monotonic increase of $\Delta E^{\ddagger}$ as a function of ω_v reflects the origin of the dynamical transition: When the temperature is very small, the kinetic energy is less than the energy barriers separating the vibrational potential wells and the motions are perfectly vibrational. In contrast, at higher temperatures the kinetic energy exceeds the energy barriers between the vibrational potential wells and thus the diffusion is enhanced, beginning with the lowest frequency vibrational modes. The magnitude of the diffusional enhancement depends on the ratio of $\Delta E^{\ddagger}$ to the kinetic energy, $k_B T/2$, and is thus greater in lower frequency vibrational modes. A sudden activation of the diffusional motions at $T \sim 180$ K is facilitated by a transition-like shift to lower frequency of the vibrational modes and thus a decrease of their corresponding $\Delta E^{\ddagger}$.

Second, the diffusion constant, D, was evaluated, leading to estimation of the diffusional contribution. From the CACF the mean-square deviation along PCA mode n, $\langle \Delta x_n^2(t) \rangle$, is calculated as

$$\langle \Delta x_n^2(t) \rangle \equiv \langle [x_n(t) - x_n(0)]^2 \rangle = 2\langle x_n^2 \rangle [1 - \psi_{coo,n}(t)] \qquad (19)$$

By use of eq 19, D_n is calculated as $D_n = \langle \Delta x_n^2(L) \rangle / 2L$, where L is a time duration long enough for the diffusion process to be sampled. Here L was set the same as the time duration used for the CACF fitting to eq 13, i.e., $L = 5-20$ ps. Applying the CACF model enables the rise of the mean-square deviation to be separated into vibrational and diffusional contributions using eq 13.

The transition probability, k, was calculated using Kramers' rate theory.[20] k is derived from the vibrational frequency and friction and the height of the vibrational potential energy barrier as

$$k = \frac{(\gamma^2/4 + \omega_{\neq}^2)^{1/2} - \gamma/2}{\omega_{\neq}} \left(\frac{\omega_v}{2\pi} \exp[-\beta \Delta E^{\ddagger}] \right) \qquad (20)$$

where $\omega_{\neq}$ is the frequency of transition barrier curvature. In this study $\omega_{\neq}$ is assumed to be equal to ω_v. Trial applications to eq 20 of other possible functions of $\omega_{\neq}$ showed little difference in k relative to $\omega_{\neq} = \omega_v$ (results not shown). Assuming the diffusion along each PCA mode n to be a random walk on a one-dimensional lattice with a separation of $a_n = \langle x_n^2 \rangle_{vib}^{1/2}$ (the associated PES is schematized in Figure 10a), D_n, is derived as[39]

$$D_n = k_n a_n^2 = k_n \langle x_n^2 \rangle_{vib} \qquad (21)$$

In panels b1−b4 in Figure 10 the diffusion constants calculated directly from the MD simulations at 300 K are compared with those derived from the CACF model (eq 19) and those from the transition probability (eq 21). For those lowest-frequency PCA modes for which $\omega_v = 0$ was obtained from the CACF fitting (eq 13), eq 12 was fitted to the VACF in order to obtain the nonzero vibrational frequencies. D from the MD is perfectly reproduced by the CACF model (with a correlation coefficient of 0.97) and reasonably well reproduced by Kramers' rate theory (with a correlation coefficient of 0.68). D from the CACF model using only the diffusional contribution (Figure 10b3) also reproduces the MD-derived diffusion constants (with a correlation coefficient of 0.95), indicating that the rise of the mean-square deviation via vibration makes little contribution to the calculation of the diffusion constant. The above results indicate that the diffusion constants can be

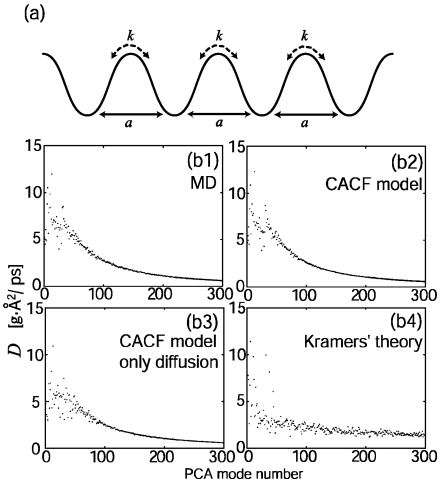

Figure 10. (a) Schematic drawing of potential energy surface for associated diffusive motion as a random walk on a one-dimensional lattice in eq 21. (b) Diffusion constant along each PCA mode as a function of PCA mode number, obtained from (1) MD trajectories, (2) CACF model (eq 19), (3) CACF model but only with diffusion term, and (4) Kramers' rate theory (eq 21). In (1−3) the time duration of 5−20 ps is used, depending on the damping time scale of the mean-square deviation of each PCA mode.

determined from the estimated heights of the vibrational energy barriers using Kramers' rate theory. Therefore, the diffusional contribution can be estimated using solely the characteristics of the vibrational potential wells.

Finally, phenomenological model functions of the CACF model parameters in eq 13 are constructed. Assuming the vibrational frequencies to be known, model functions of the vibrational friction, γ_v, vibrational fraction, κ, and diffusional damping coefficient, γ_0, were constructed as a function of ω_v. Here the results from the MD trajectory at 300 K are shown: similar model functions were also derived at different temperatures.

The vibrational friction, γ_v, was modeled in the previous section as $\gamma_v = A\omega_v + \Delta\gamma$ with $A = 0.375$ and $\Delta\gamma = 1.98$ (ps^{-1}) at 300 K.

The vibrational fraction, κ, is assumed to increase with $\Delta E^{\ddagger}$. The resulting model function at 300 K is $1 - \kappa = \exp(a/\Delta E^{\ddagger 2} - b)$ with $a = 3.13 \times 10^5$ (J^2) and $b = 1.06$.

The mean-square fluctuation, $\langle x^2 \rangle$, was modeled using the vibrational MSF under the equilibrium condition at a temperature of T as

$$\langle x^2 \rangle = \frac{\langle x^2 \rangle_{vib}}{\kappa} = \frac{k_B T}{\omega_v{}^2 \kappa} \tag{22}$$

The diffusion damping coefficient, γ_0, was modeled from the estimated diffusion constant discussed previously. Matching the diffusion constants derived from eqs19 and 21 gives

$$D_n = k_n \langle x_n{}^2 \rangle_{vib} = \frac{\langle x_n{}^2 \rangle [1 - \psi_{coo,n}(L)]}{L} \tag{23}$$

When $L = 2/\gamma_0$ (which is enough long for the diffusion process) is applied to eq 23 and only the diffusion element is used for the CACF in eq 13, γ_0 is modeled as

$$\gamma_0 = \frac{4k\kappa}{(1 - \kappa)(1 - e^{-2})} \tag{24}$$

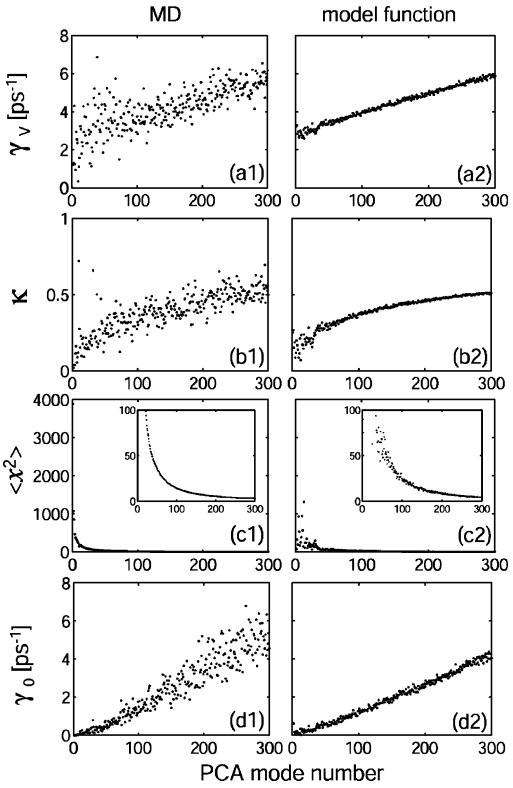

Figure 11. CACF model parameters at 300 K derived from (1) MD-derived and (2) model parameter functions are plotted as a function of PCA mode number: (a) vibrational friction, (b) vibrational fraction, (c) mean-square fluctuation (eq 22), and (d) diffusion damping coefficient (eq 24).

Figure 11 compares the MD-derived and model parameters at 300 K, indicating good agreement (the correlation coefficients are 0.78, 0.76, 0.40, and 0.93 for γ_v, κ, $\langle x^2 \rangle$, and γ_0, respectively). Therefore, the simplified model functions are useful for representing protein dynamics in combination with the present CACF model.

3.4. Dynamic Structure Factor. Finally, we now compared the dynamic structure factor, $S(q,\omega)$, derived directly from the MD simulations (calculated using eqs 14 and 15) with spectra calculated from the CACF model (eq 13) using the MD-derived or model parameters (calculated using eqs 14 and 16). Furthermore, the validity of the model functions of parameters discussed above (e.g., eqs 22 and 24) was examined by comparing the spectra obtained using them.

In Figure 12 is shown $S(q,\omega)$ calculated directly from the MD trajectory in solution at 300 K together with those derived from the VACF model (eq 12) and the CACF model (eq 13) with the MD-derived parameters. The CACF model reproduces excellently both the vibrational (∼1−60 meV, inelastic) and diffusive (<1 meV, quasielastic) region of the MD spectrum. In contrast, the spectrum from the VACF model lacks quasielastic intensity in the region ∼0.1−0.5 meV, i.e., the contribution of the diffusive, slow motions. These results further confirm the validity of the CACF model, in which the motion along each PCA mode takes place via a sequence of vibrational potential wells on a flat potential energy surface.

Finally, Figure 12 also shows that $S(q,\omega)$ calculated from the model functions of the CACF model parameters also reproduces the MD spectra. Thus, the dynamic structure factor can be reproduced by the CACF model with the simplified model parameters as a function of vibrational frequency of each vibrational mode.

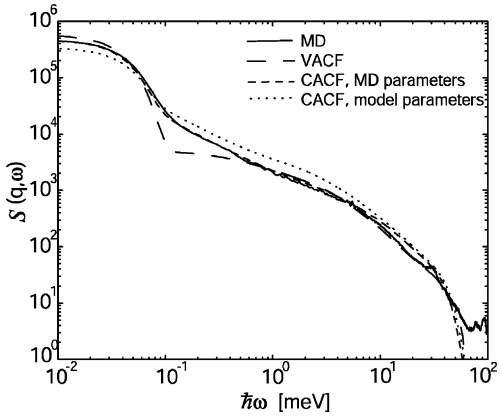

Figure 12. Dynamic structure factor, $S(q,\omega)$, at $q = 2$ Å^{-1} and $T =$ 300 K (see text), derived from MD trajectory (thick solid curve), from CACF model in eq 13 with MD-derived parameters (dashed curve) and with model parameters (e.g., eqs 22 and 24) (dotted curve), and from the VACF model in eq 12 with MD-derived parameters (thin solid curve).

4. Conclusion

In this paper internal protein dynamics is represented using a model combining Langevin vibration with diffusion. This is achieved by modeling the coordinate autocorrelation function in combination with principal component analysis, using molecular dynamics trajectories of myoglobin at various temperatures. The model parameters obtained, i.e., the vibrational frequency and friction, the diffusion damping constant, and the vibrational fraction, characterize the potential energy surface (schematized in Figure 1). The temperature dependence of protein anharmonic motion is examined through these model parameters, allowing physical insight into dynamical-transition phenomena to be obtained.

Comparison between the coordinate and velocity autocorrelation functions of selected principal components from the MD trajectories demonstrates that the diffusive dynamics appears only in the CACF. The MD-derived CACF is well described by the model of the Langevin vibration combined with simple diffusion. The PCA decomposition into individual components, each with one characteristic time scale, facilitates the application of this simple model. The description of diffusion with a single exponential is appropriate for analyzing protein dynamics on the present time scale of ~1 ns. This is consistent with a previous protein MD analysis in which the slow motion, along the largest-amplitude PCA modes, was found to resemble simple diffusion on a flat potential energy surface.[40,41] However, more complicated diffusive motion may be expected to appear on longer time scales. Modeling of the MD-derived mean-square displacement has shown that a combination of simple diffusive motion with various diffusion constants represents well protein internal diffusion on time scales longer than ~1 ns,[42,43] suggesting a possible extension of the present model by the addition of exponential terms to eq 13. Furthermore, in long time scale, converged MD trajectories, slow, diffusive motion may also eventually appear in the VACF or its memory function.[8]

The long-time dynamics is not well sampled in the present simulations, and the significant sine wave content of the PCA coordinate in Figure 3 shows that the present MD simulations have not converged.[40,41] However, the effect of this sine-wave artifact was avoided in the present study by fitting the CACF to only short time scale 5 − 20 ps dynamics, much shorter than the period of the sine wave, which is >~100 ps. Nevertheless, the dynamic structure factor from the 1-ns MD trajectories is well reproduced by the model, in which the long-time scale behavior of the CACF is simplified by applying a single-exponential approximation for the slow protein internal diffusion. Trial longer MD simulations of 10 ns at 300 K resulted in the obtention of smaller values for γ_0 and κ, consistent with longer time scale dynamics and larger diffusional amplitudes being observed in the longer MD simulations (results not shown). Thus, the parameters derived do change with the MD simulation length. However, at both time scales the model was found to reproduce the motion concerned, and the calculated $S(q,\omega)$ was not significantly different (results not shown).

The model parameters were used to probe the temperature dependence of protein dynamics. The vibrational frequency, ω_v, quantifying the curvature of the potential wells, is smaller for the larger-amplitude principal components. ω_v decreases with temperature, due to PES broadening arising from the anharmonicity.[9] This is consistent with the common observation that the curvature of vibrational potential wells often becomes broader with increasing vibrational amplitudes. A transition is clearly seen at the glass-transition temperature, reflecting a rapid increase of anharmonicity. The vibrational friction, γ_v, characterizing the roughness of the potential wells, increases with ω_v in accordance with stronger resonance coupling to protein high-frequency vibrations.[9,37,38] γ_v increases linearly with temperature, independent of the dynamical transition, i.e., of the activation of the diffusive motions.

The vibrational fraction, κ, increases continuously with decreasing PCA amplitude, in contrast to the behavior seen in the deterministic descriptions of the previous studies.[6,30] The dynamical transition behavior involves a rapid enhancement of diffusion between vibrational potential wells. The diffusional mean-square fluctuation undergoes a dynamical transition, independent of the linear increase of the vibrational MSF. This result clarifies the fact that the sudden increase of the MSF is due to the onset of diffusion at the glass-transition temperature, aspects of which have been discussed in relation to both experiment[17−19] and computer simulation.[32,33,44−46]

Using the present model, the heights of energy barriers between the vibrational potential wells, $\Delta E^{\ddagger}$, were estimated. This is possible by assuming that the vibrational potential wells are approximated as harmonic and their amplitudes are fully explored in the cases where diffusive motions between the vibrational potential wells exist. The heterogeneity over PCA modes originating from the complex structure of the real potential energy surface results in the spread distribution of $\Delta E^{\ddagger}$ as a function of vibrational frequency. However, in the present study a fitting function, which allows such heterogeneity to be averaged out, was used for the analysis. This fitting function enables finally the diffusion constant to be predicted using the model, supporting the validity of this rough assumption of the vibrational potential wells.

$\Delta E^{\ddagger}$ increases roughly linearly as a function of the vibrational frequency. This indicates that lower-frequency motions, on broader potentials, are more likely to cross energy barriers and undergo diffusion than higher-frequency motions, revealing the origin of the protein dynamical transition. Knowledge of $\Delta E^{\ddagger}$, combined with the vibrational frequencies and frictions, allows the transition probability to be calculated using Kramers' rate theory, leading to estimation of the associated diffusion constant. The diffusion constant thus obtained is in good agreement with that calculated directly from the MD. Therefore, the present modeling allows the diffusional contribution to be estimated simply using the vibrational frequencies.

Model functions of parameters were constructed for the present CACF model. The vibrational friction is well reproduced using a linear function of the vibrational frequencies. Furthermore, diffusion-related parameters, i.e., the vibrational fraction and the diffusion damping coefficient, can also be described by simple functions of only the vibrational frequencies, with the help of the estimated diffusion constants. Therefore, the present CACF model and the model functions obtained, where combined with the vibrational motions and their frequencies, allow many aspects of protein internal dynamics to be reproduced. The dynamic structure factors were calculated to test the validity of the present model and its model parameter functions obtained. $S(q,\omega)$ calculated directly from the MD trajectories was compared with those from the present CACF and the VACF models. The CACF model reproduces the MD spectra perfectly, whereas, in contrast, the VACF model underestimates the quasielastic intensity arising from the slow, diffusive motion. The spectra from the CACF model with the model functions of parameters are also in good agreement with the MD spectra, confirming the validity of these simplified model parameters combined with the CACF model.

The present model requires the vibrational motions as input. Normal-mode analysis is a common method for obtaining a set of vibrational motions with their frequencies and their atomic displacement vectors. The possibility of further simplification may exist by using a vibrational model in which the potential energy is approximated as the sum of Hookean pairwise harmonic potentials between atom pairs within an arbitrary cutoff distance.[47−51]

Further development of the present model may be envisaged, for example, by representing diffusion using a more complicated function and/or by adding a coupling term between the vibration and diffusion. Furthermore, work is in progress improving the model parameter functions and analyzing their coefficients as a function of temperature so as to obtain further understanding of temperature-dependent protein dynamics. However, the dynamical model proposed herein, simplifying the motion of each principal component as Langevin vibration combined with simple diffusion, is likely to be of general use for understanding protein internal dynamics and the underlying potential energy surface and can also be used to interpret experiments, such as quasielastic neutron scattering.[19,34,52−55]

Acknowledgment. K.M. acknowledges a research fellowship of the Japan Society of the Promotion of Science (JSPS) for young scientists. Simulations were performed on the HELICS supercomputer at the Interdisciplinary Center for Scientific Computing (IWR) in University of Heidelberg.

References and Notes

(1) Frauenfelder, H.; Sligar, S. G.; Wolynes, P. G. *Science* **1991**, *254*, 1598.
(2) Frauenfelder, H.; Parak, F.; Young, R. D. *Annu. Rev. Biophys. Biophys. Chem.* **1988**, *17*, 451.
(3) Karplus, M.; McCammon, J. A. *Nat. Struct. Biol.* **2002**, *9*, 646.
(4) Amadei, A.; Linssen, A. B. M.; Berendsen, H. J. C. *Proteins* **1993**, *17*, 283.
(5) de Groot, B. L.; van Aalten, D. M. F.; Amadei, A.; Berendsen, H. J. C. *Biophys. J.* **1996**, *71*, 1707.
(6) Kitao, A.; Hayward, S.; Go, N. *Proteins* **1998**, *33*, 496.
(7) Kitao, A.; Go, N. *Curr. Opin. Struct. Biol.* **1999**, *9*, 164.
(8) Boon J. P.; Yip S. *Molecular Hydrodynamics*; Dover Publications, Inc.; New York, 1991.
(9) Moritsugu K.; Smith J. C. *J. Phys. Chem. B* **2005**, *109*, 12182.
(10) Lamm, G.; Szabo, A. *J. Chem. Phys*. **1986**, *85*, 7334.
(11) Kottalam, J.; Case, D. A. *Biopolymers* **1990**, *29*, 1409.
(12) Kitao, A.; Hirata, F.; Gô, N. *Chem. Phys*. **1991**, *158*, 447.
(13) Hayward, S.; Kitao, A.; Hirata, F.; Go, N. *J. Mol. Biol*. **1993**, *234*, 1207.
(14) Ansari, A. *J. Chem. Phys*. **1999**, *110*, 1774.
(15) Kneller, G. R. *Chem. Phys*. **2000**, *261*, 1.
(16) Hinsen, K.; Petrescu, A. J.; Dellerue, S.; Bellissent-Funel, M. C.; Kneller, G. R. *Chem. Phys.* **2000**, *261*, 25.
(17) Parak, F.; Formanek, H. *Acta Crystallogr., Sect. A* **1971**, *27*, 573.
(18) Iben, I. E.; Braunstein, D.; Doster, W.; Frauenfelder, H.; Hong, M. K.; Johnson, J. B.; Luck, S.; Ormos, P.; Schulte, A.; Steinbach, P. J.; Xie, A. H.; Young, R. D. *Phys. Rev. Lett*. **1989**, *62*, 1916.
(19) Doster, W.; Cusack, S.; Petry W. *Nature* **1989**, *337*, 754.
(20) Kramers H. A. *Physica* **1940**, *7*, 284.
(21) Vojtechovsky, R.; Chu, K.; Berendzen, J.; Sweet, R. M.; Schlichting, I. *Biophys. J.* **1999**, *78*, 2752.
(22) Jorgensen, W. D.; Chandrasekhar, J.; Madura, J. D. *J. Chem. Phys.* **1983**, *79*, 926.
(23) Brooks, B. R.; Bruccoleri, R. E.; Olafson, B. D.; States, D. J.; Swaminathan, S.; Karplus, M. *J. Comput. Biol*. **1983**, *4*, 187.
(24) MacKerell, A. D., Jr.; Bashford, D.; Bellott, R. L.; Dunbrack, R. L., Jr.; Evanseck, J. D.; Field, M. J.; Fischer, S.; Gao, J.; Guo, H.; Ha, S.; Joseph-McCarthy, D.; Kuchnir, L.; Kuczera, K.; Lau, F. T. K.; Mattos, C.; Michnick, S.; Ngo, T.; Nguyen, D. T.; Prodhom, B.; Reiher, W. E., III.; Roux, B.; Schlenkrich, M.; Smith, J. C.; Stote, R.; Straub, J.; Watanabe, M.; Wiorkiewicz-Kuczera, J.; Yin, D.; Karplus, M. *J. Phys. Chem. B* **1998**, *102*, 3586.
(25) Darden, T. A.; York, D. M.; Pederson, L. G. *J. Chem. Phys*. **1993**, *98*, 10089.
(26) Essmann, U.; Perera, L.; Berkowitz, M. L.; Darden, T. A.; Pederson, L. G. *J. Chem. Phys.* **1995**, *103*, 8577.
(27) Noœe, S. *Mol. Phys.* **1984**, *52*, 255.
(28) Hoover, W. G. *Phys. Rev. A* **1985**, *31*, 1695.
(29) Chandrasekhar, S. *Rev. Mod. Phys.* **1943**, *15*, 1.
(30) Tournier, A. L.; Smith, J. C. *Phys. Rev. Lett.* **2003**, *91*, 208106.
(31) Kneller, G. R.; Smith, J. C. *J. Mol. Biol.* **1994**, *242*, 181.
(32) Hayward, J. A.; Smith, J. C. *Biophys. J*. **2002**, *82*, 1216.
(33) Hayward, J. A.; Finney, J. L.; Daniel, R. M.; Smith, J. C. *Biophys. J*. **2003**, *85*, 679.
(34) Diehl, M.; Doster, W.; Petry, W.; Schober, H. *Biophys. J.* **1997**, *73*, 2726.
(35) Robertson, G. N.; Yarwood, J. *Chem. Phys*. **1978**, *32*, 267.
(36) Smith, J. C.; Cusack, S.; Tidor, B.; Karplus, M. *J. Chem. Phys*. **1990**, *93*, 2974.
(37) Moritsugu, K.; Miyashita, O.; Kidera, A. *Phys. Rev. Lett.* **2000**, *85*, 3970.
(38) Moritsugu, K.; Miyashita, O.; Kidera, A. *J. Phys. Chem. B* **2003**, *107*, 3309.
(39) McQuarrie D. A. *Statistical Mechanics*; Harper and Row: New York, 1976.
(40) Hess, B. *Phys. Rev. E* **2000**, *62*, 8438.
(41) Hess, B. *Phys. Rev. E* **2002**, *65*, 031910.
(42) Amadei, A.; de Groot, B. L.; Ceruso, M. A.; Paci, M.; Di Nola, A.; Berendsen, H. J. C. *Proteins*: *Struct. Funct. Genet*. **1999**, *35*, 283.
(43) Daidone, I.; Amadei, A.; Di Nola, A. *Proteins*: *Struct. Funct. Genet.* **2005**, *59*, 510.
(44) Smith J. C.; Kuczera K.; Karplus, M. *Proc. Natl. Acad. Sci. U.S.A.* **1900**, *87*, 1601.
(45) Kneller, G.; Smith J. C. *J. Mol. Biol*. **1994**, *242*, 181.
(46) Becker, T.; Hayward, J. A.; Finney, J. L.; Daniel, R. M.; Smith, J. C. *Biophys. J.* **2004**, *87*, 1436.
(47) Tirion, M. M. *Phys. Rev. Lett.* **1996**, *77*, 1905.
(48) Hinsen, K. *Proteins*: *Struct. Funct. Genet.* **1998**, *33*, 417.
(49) Tama, F.; Brooks, C. L., III *J. Mol. Biol*. **2002**, *318*, 733.
(50) Tama, F.; Wriggers, W.; Brooks, C. L., III *J. Mol. Biol*. **2002**, *321*, 297.
(51) Tama, F. *Protein Pept. Lett.* **2003**, *10*, 119.
(52) Cusack, S.; Doster, W. *Biophys. J.* **1990**, *58*, 243.
(53) Smith, J. C. *Q. Rev. Biophys*. **1991**, *24*, 227.
(54) Fitter, J.; Lechner, R. E.; Bueldt, G.; Dencher, N. A. *Proc. Natl. Acad. Sci. U.S.A.* **1996**, *93*, 7600.
(55) Paciaroni, A.; Bizzarri, A. R.; Cannistraro, S. *J. Mol. Liq.* **2000**, *84*, 3.